Quantum and classical criticality in a dimerised quantum antiferromagnet

P. Merchant,[1] B. Normand,[2] K. W. Krämer,[3] M. Boehm,[4] D. F. McMorrow,[1] and Ch. Rüegg[1,5,6]

[1]*London Centre for Nanotechnology and Department of Physics and Astronomy, University College London, London WC1E 6BT, UK*
[2]*Department of Physics, Renmin University of China, Beijing 100872, China*
[3]*Department of Chemistry and Biochemistry, University of Bern, CH–3012 Bern 9, Switzerland*
[4]*Institut Laue Langevin, BP 156, 38042 Grenoble Cedex 9, France*
[5]*Laboratory for Neutron Scattering, Paul Scherrer Institute, CH–5232 Villigen, Switzerland*
[6]*DPMC–MaNEP, University of Geneva, CH–1211 Geneva, Switzerland*

(Dated: January 20, 2014)

A quantum critical point (QCP) is a singularity in the phase diagram arising due to quantum mechanical fluctuations. The exotic properties of some of the most enigmatic physical systems, including unconventional metals and superconductors, quantum magnets, and ultracold atomic condensates, have been related to the importance of the critical quantum and thermal fluctuations near such a point. However, direct and continuous control of these fluctuations has been difficult to realise, and complete thermodynamic and spectroscopic information is required to disentangle the effects of quantum and classical physics around a QCP. Here we achieve this control in a high-pressure, high-resolution neutron scattering experiment on the quantum dimer material $TlCuCl_3$. By measuring the magnetic excitation spectrum across the entire quantum critical phase diagram, we illustrate the similarities between quantum and thermal melting of magnetic order. We prove the critical nature of the unconventional longitudinal ("Higgs") mode of the ordered phase by damping it thermally. We demonstrate the development of two types of criticality, quantum and classical, and use their static and dynamic scaling properties to conclude that quantum and thermal fluctuations can behave largely independently near a QCP.

In "classical" isotropic antiferromagnets, the excitations of the ordered phase are gapless spin waves emerging on the spontaneous breaking of a continuous symmetry[1]. The classical phase transition, occurring at the critical temperature T_N, is driven by thermal fluctuations. In quantum antiferromagnets, quantum fluctuations suppress long-range order, and can destroy it completely even at zero temperature[2]. The ordered and disordered phases are separated by a quantum critical point (QCP), where quantum fluctuations restore the broken symmetry and all excitations become gapped, giving them characteristics fundamentally different from the Goldstone modes on the other side of the QCP (Fig. 1). At finite temperatures around a QCP, the combined effects of quantum and thermal fluctuations bring about a regime where the characteristic energy scale of spin excitations is the temperature itself, and this quantum critical (QC) regime has many special properties[3].

Physical systems do not often allow the free tuning of a quantum fluctuation parameter through a QCP. The QC regime has been studied in some detail in heavy-fermion metals with different dopings, where the quantum phase transition (QPT) is from itinerant magnetic phases to unusual metallic or superconducting ones[4–6], in organic materials where a host of insulating magnetic phases become (super)conducting[7,8], and in cold atomic gases tuned from superfluid to Mott-insulating states[9,10]. However, the dimerised quantum spin system $TlCuCl_3$ occupies a very special position in the experimental study of QPTs. The quantum disordered phase at ambient pressure and zero field has a small gap to spin excitations. An applied magnetic field closes this gap, driving a QPT to an ordered phase, a magnon condensate in the Bose-Einstein universality class, with a single, nearly massless excitation[11,12].

Far more remarkably, an applied pressure also drives a QPT to an ordered phase[13], occurring at the very low critical pressure $p_c = 1.07$ kbar[14] and sparking detailed studies[15,16]. This ordered phase is a different type of condensate, whose defining feature is a massive excitation, a "Higgs boson" or longitudinal fluctuation mode of the weakly ordered moment[17,18]. This excitation, which exists alongside the two transverse (Goldstone) modes of a conventional well-ordered magnet, has been characterised in detail by neutron spectroscopy with continuous pressure control through the QPT[19] and subsequently by different theoretical approaches[20,21]. $TlCuCl_3$ is therefore an excellent system for answering fundamental questions about the development of criticality, the nature of the QC regime, and the interplay of quantum and thermal fluctuations by controlling both the pressure and the temperature.

Here we present inelastic neutron scattering (INS) results which map the evolution of the spin dynamics of $TlCuCl_3$ throughout the quantum critical phase diagram in pressure and temperature. The spin excitations we measure exhibit different forms of dynamical scaling behaviour arising from the combined effects of quantum and thermal fluctuations, particularly on crossing the QC regime and at the line of phase transitions to magnetic order (Fig. 1). To probe these regions, we collected spectra up to 1.8 meV for temperatures between $T = 1.8$

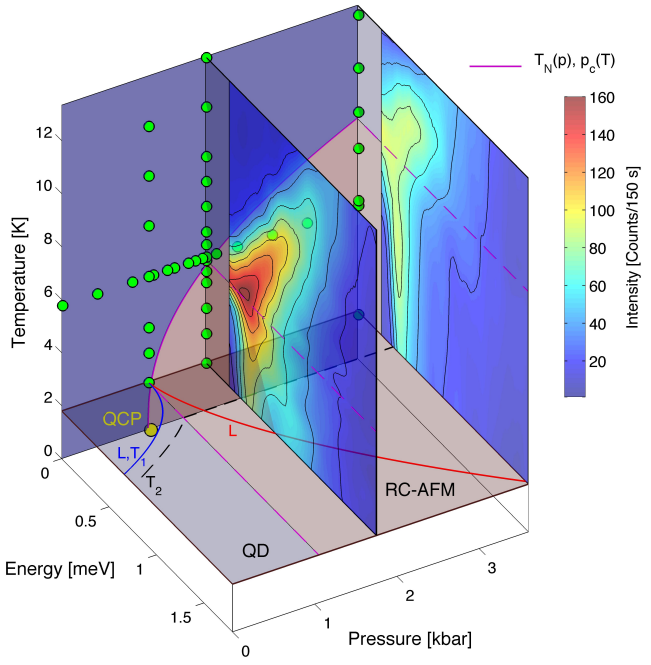

FIG. 1: Pressure-temperature phase diagram of $TlCuCl_3$ extended to finite energies, revealing quantum and thermal critical dynamics. The rear panel is the bare (p, T) phase diagram at energy $E = 0$ meV, in which the magenta line shows the Néel temperature as a function of pressure, $T_N(p)$[14], and the green points depict the temperature and pressure values studied. Full details of this panel are presented in Fig. 4(c). The centre (E, T) panel shows neutron intensity data collected from $T = 1.8$ K to 12.7 K at $p = 1.75$ kbar, where $T_N = 5.8$ K. The rightmost (E, T) panel shows the corresponding data at $p = 3.6$ kbar, where $T_N = 9.2$ K. The data in both (E, T) panels display a clear softening of the magnetic excitations at $T_N(p)$. The bottom (p, E) panel indicates the softening of the excitations, measured at $T = 1.8$ K, across the QPT[19]. T_1, T_2 and L denote the three gapped triplet excitations of the quantum disordered (QD) phase. In the renormalised classical antiferromagnetic (RC-AFM) ordered phase, these become respectively the gapless Goldstone mode, which is a transverse spin wave, a gapped (anisotropic) spin wave, and the longitudinal "Higgs" mode (see text).

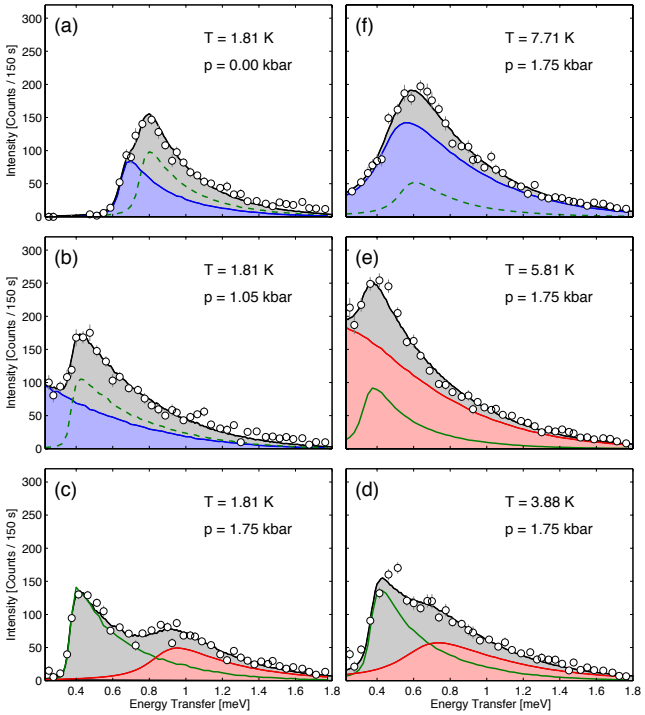

FIG. 2: INS spectra collected at $\mathbf{Q} = (0\ 4\ 0)$ r.l.u., the wavevector of the minimum energy gap in the QD phase, where magnetic order is induced with increasing pressure. (a-c) Evolution of triplet excitations during pressure-induced magnetic ordering, as the lower mode (L and T_1, blue) changes continuously into the longitudinal mode (L, red), while the anisotropic mode (T_2, green) remains gapped. (d-f) Evolution as increasing temperature lowers the longitudinal-mode gap to zero at $T = 5.8$ K, above which all three modes are gapped in a disordered (QC) state. Error bars mark statistical uncertainties in the intensity measurements.

K and 12.7 K, and over a range of applied hydrostatic pressures. Our measurements were performed primarily at $p = 1.05$ kbar ($\simeq p_c$ at the lowest temperatures), 1.75 kbar, and 3.6 kbar, and also for all pressures at $T = 5.8$ K. Most measurements were made at the ordering wavevector, $\mathbf{Q}_0 = (0\ 4\ 0)$ reciprocal lattice units (r.l.u.), and so concern triplet mode gaps. From the INS selection rules, only one transverse mode of the ordered phase is observable at $\mathbf{Q} = \mathbf{Q}_0$, and it is gapped ($\Delta_{T2} = 0.38$ meV) due to a 1% exchange anisotropy[19]. These features allow an unambiguous separation of the intensity contributions from modes of each transverse or longitudinal polarisation[19]. In the summary presented in Fig. 1, the contours represent scattered intensities at two selected pressures $p > p_c$. Both panels show strong QC scattering and a nontrivial evolution of the mode gaps and spectral weights with both p and T, which is quantified in Fig. 2.

Figures 2(a-c) show respectively the measured intensities for pressures below, at, and above the QPT at a fixed low temperature. Fits to the lineshapes of the separate excitations were made by a resolution deconvolution requiring both the gap and the local curvature of the mode dispersion, which was taken from a finite-temperature bond-operator description[22,23]. The distinct contributions from transverse and longitudinal fluctuations change position systematically as the applied pressure induces magnetic order. The intensity of the longitudinal mode is highlighted in red in Fig. 2(c). Figures 2(d-f) show respectively the measured intensities for temperatures below, at, and above the phase transition $[T_N(p)]$ at a fixed pressure $p > p_c$. Quantitatively, the intensity and the linewidth increase from the left to the right panels due to the temperature. Qualitatively, the thermal evolution is almost exactly analogous to a change in the pressure, with the spectral weight of the longitu-

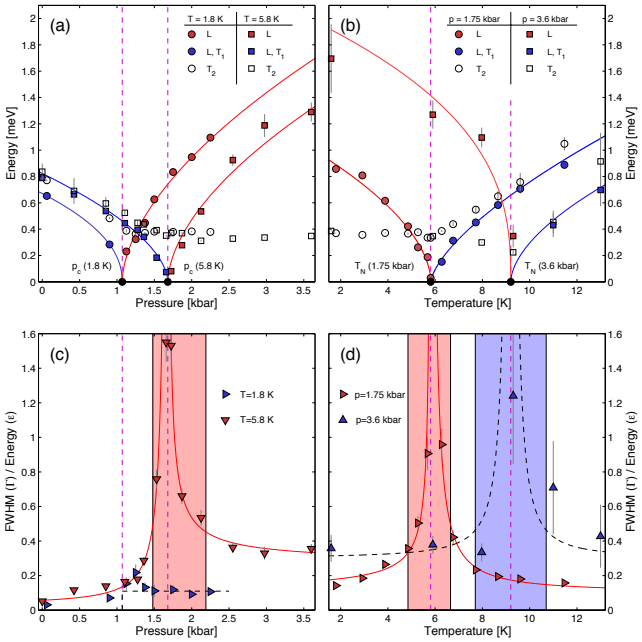

FIG. 3: Spin dynamics at the quantum and thermal "melting" transitions. (a) Quantum melting of magnetic order, shown by the triplet gaps for two different temperatures ($T = 1.8$ and 5.8 K), occurs from right to left. (b) Thermal melting, shown for two different pressures ($p = 1.75$ kbar and 3.6 kbar), occurs from left to right. Open black circles and squares give the energies of the anisotropic transverse excitations (T_2), which remain gapped, while filled circles and open squares show the longitudinal mode (red in the ordered phase, blue in the disordered one). The lines are power-law fits, described in the text. (c,d) Linewidth-to-energy ratios $\Gamma_{\mathbf{Q}}/\epsilon_{\mathbf{Q}}$ for the longitudinal mode across the phase transition as a function of pressure at $T = 1.8$ and 5.8 K (c) and of temperature at $p = 1.75$ and 3.6 kbar (d); lines are guides to the eye and shaded regions are explained in the text. Error bars in all panels mark fitting uncertainties in the resolution deconvolution procedure.

dinal mode softening at $T_N(p = 1.75\ \text{kbar}) = 5.8$ K but moving again to finite energies at temperatures above T_N.

We analyze these results in detail by extracting the excitation energies $\epsilon_{\mathbf{Q}}$ and linewidths $\Gamma_{\mathbf{Q}}$ from the data of Fig. 2. Figure 3(a) shows the evolution of the mode gaps ($\epsilon_{\mathbf{Q}=\mathbf{Q}_0}$) with pressure for $T = 1.8$ K (the QPT, *cf.* Ref. 19) and $T = 5.8$ K. The longitudinal mode of the ordered phase appears on the right, and softens with decreasing pressure until $p_c(T)$. The Goldstone mode is not visible due to the scattering geometry. At pressures below $p_c(T)$, the effect of dimer-based quantum fluctuations is to destroy the magnetic order and gap all the modes. The lines are best fits to power laws of the form $\Delta(p) = A|p - p_c|^{\gamma_p}$, which we discuss below.

Figure 3(b) shows the evolution of the mode gaps over the temperature range 1.8 K $< T <$ 12.7 K for pressures $p = 1.75$ kbar and 3.6 kbar. Here the ordered phase is on the left, where the longitudinal mode, which dominates the low-energy scattering around the critical point, becomes soft at a Néel temperature $T_N(p)$ determined by the pressure. They reemerge on the right as gapped triplets of the thermally disordered QC phase. The lines in this figure are best fits to power laws of the form $\Delta(T) = B|T - T_N|^{\gamma_T}$. The similarity between quantum and thermal melting shown in Figs. 2 and 3 is a remarkable result. It is essential to note that the disorder in Fig. 3(b) is thermal, and not due to quantum fluctuations. Thermal fluctuations in a quantum dimer system, whose triplet excitations are hard-core bosons, do not simply broaden and damp the modes of the ordered magnet, but cause a very specific and systematic evolution of the spectral weight[22]. On the ordered side, the massive, longitudinal mode becomes gapless at the classical phase transition, while on the disordered side there is not merely a featureless paramagnet but a clear gapped excitation. This is also the case for the pressure-driven transition at finite temperatures [Fig. 3(a)], where the symmetry is restored before all three excitations become gapped modes of the QC phase.

Figures 3(c) and (d) show the linewidths of the longitudinal mode, measured respectively through the quantum and thermal transitions, in the form of the ratio $\Gamma_{\mathbf{Q}}/\epsilon_{\mathbf{Q}} = \alpha_L$. For the pressure-induced phase transition in Fig. 3(c), the ratio vanishes at $T = 1.8$ K for the well-defined excitations on the disordered side and remains constant (with $\alpha_L \simeq 0.15$) on the ordered side of the QCP, demonstrating its critically damped nature[19]. However, this is not at all the case at $T = 5.8$ K, where the divergence of $\alpha_L(T)$ shows the longitudinal mode becoming overdamped in the presence of thermal fluctuations. For the thermally driven phase transition at $p = 1.75$ and 3.6 kbar [Fig. 3(d)], the ratio also diverges on approaching the critical temperature $T_N(p)$.

The QC regime is the area around the line $p = p_c$ where the intrinsic energy scale of the system (the gap Δ in the QD phase, or T_N in the ordered phase[2]) is lower than the temperature[3]. Near p_c, the measured neutron intensities [Fig. 4(a)] show a broad range over which spin excitations are present, with a peak along a line corresponding approximately to $\hbar\epsilon_{\mathbf{Q}} = k_{\mathrm{B}}T$. This "$\omega/T$" scaling property[3] is evident in the self-similar nature of the spectra at different temperatures. The QCP is the point where the intrinsic energy scale vanishes, and thus states become available at all energies; it is the maximum in their occupation that scales with T, and hence the temperature becomes the new characteristic energy scale. The microscopic origin of this "thermal gap" in the measured spectrum is mutual blocking of the hard-core triplet excitations[22]. As shown in Fig. 4(b), the linewidth $\Gamma_{\mathbf{Q}} = \alpha_c\epsilon_{\mathbf{Q}}$ also scales linearly with T, illustrating that critical damping is an essential property of QC excitations. We draw attention to the fact that these QC excitations are remarkably narrow, with $\alpha_c \simeq 0.14$ taking a value similar to that for the Higgs mode of the ordered phase and remaining constant to the highest temperatures measured. Narrow triplet excitations have also

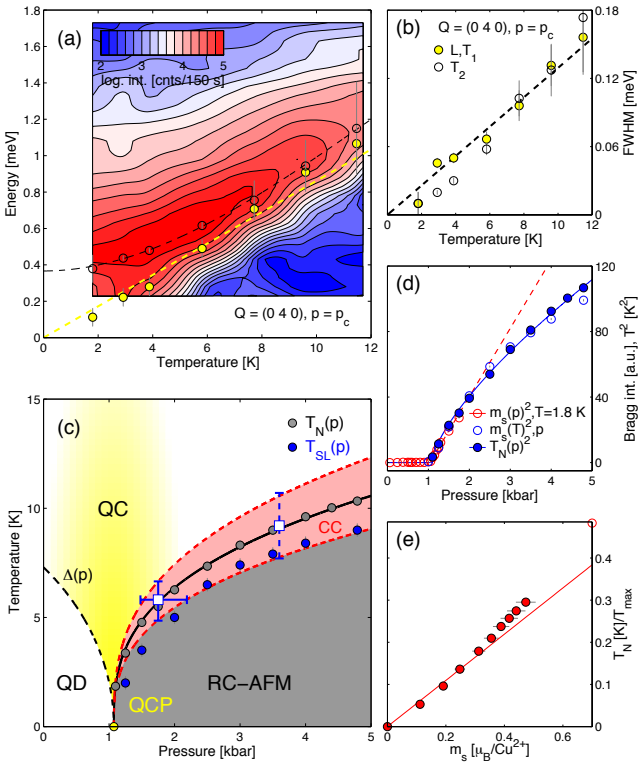

FIG. 4: Quantum and classical criticality. (a) Scattered neutron intensity at $p = p_c$ as a function of temperature. Points show the energies $\epsilon_{\mathbf{Q}}$ extracted from the intensity for the modes becoming gapless (L and T_1, yellow) and gapped (T_2, black) as $T \to 0$. (b) $\Gamma_{\mathbf{Q}}$ as a function of T at $p = p_c$. Error bars in (a) and (b) indicate uncertainties in the resolution deconvolution. (c) Complete experimental phase diagram, showing quantum disordered (QD), quantum critical (QC), classical critical (CC), and renormalised classical (RC-AFM) phases. The dashed lines denote energy scales marking crossovers in behaviour. Grey symbols denote $T_N(p)$[14], blue symbols labelled $T_{SL}(p)$ show the limit of classical critical scaling in the data for the staggered magnetisation, $m_s(T)$, and the blue bars are taken from $\Gamma_{\mathbf{Q}}/\epsilon_{\mathbf{Q}}(T)$ (see text). (d) Linear proportionality of the measured $T_N(p)$ and $m_s(p)$[14]. (e) Scaling of T_N and m_s, including one high-p data point taken from Ref. 25 for an absolute calibration of m_s. Data for m_s are normalised by $T_{max} = 35$ K, the maximum of the magnetic susceptibility[13,16]. Red lines in panels (d) and (e) represent scaling behaviour discussed in the text and error bars arise from statistical uncertainties in the intensity measurements determining m_s.

been found both analytically and numerically in the QC regime of the bilayer Heisenberg model[24].

The experimental phase diagram is shown in Fig. 4(c), and contains all four regions characteristic of the QCP[3,4]. Between the quantum disordered and renormalised classically ordered regimes[2], the dominant behaviour is QC (ω/T) scaling. On the line of classical phase transitions, the intrinsic energy scale is $T_N(p)$ but the excitation energy is driven to zero. This results in the properties, in particular the static scaling relations, of a classical critical (CC) regime. We show below that the scaling exponents in the QC and CC regions have approximately the values expected theoretically. However, for a real system such as $TlCuCl_3$, they can differ over broad crossover regions determined by the relative size of the intrinsic and excitation energy scales, and departures from universal behaviour may also arise due to microscopic details of the Hamiltonian.

We begin the analysis of our results not with static exponents but with the dynamical ones extracted from the power-law fits to the gaps in Figs. 3(a) and (b). At the pressure-controlled transition, all of the exponents we measure fall in the range $0.46(6) \leq \gamma_p \leq 0.57(6)$, which within experimental error is $\gamma_p = 1/2$. This is the mean-field expectation in the generic case that the p-dependence of the exchange parameters $J_{ij}(p)$ is predominantly linear[19]. It applies both for the disordered phase (Δ_{QD}) and for the gap (Δ_L) of the longitudinal mode, with a multiplicative prefactor $\Delta_L = \sqrt{2}\Delta_{\rm QD}$ at $T = 0$[26]. At higher temperatures we find no strong departures from universality in this exponent. However, fits including data points at the higher energies are generally less reliable, suggesting that these begin to depart from the universal regime.

For the classical (temperature-controlled) phase transition, the expectation for the QC phase is $\Delta \propto \xi^{-1} \propto (T - T_N)^{\nu}$, where $\nu \simeq 0.67$ for an XY spin symmetry and 0.70 for SU(2)[27]. The 1% exchange anisotropy in $TlCuCl_3$ reduces the spin symmetry from SU(2) to XY below energy scales of order 5 K. Our data for γ_T at $p = 1.75$ kbar give $\gamma_T = 0.67(9)$, in excellent agreement with either of these exponents but certainly unable to make the subtle distinction between them; at $p = 3.6$ kbar we do not have sufficient data for a reliable fit. At $p = p_c$, however, we find the expected QC scaling form $\gamma_T = 1$, and the width of the crossover regime remains an open question. Deducing a scaling exponent γ_T for the T-dependence of the longitudinal mode gap in the ordered phase remains a theoretical challenge. For this it is important to recall that at finite temperature this Higgs mode becomes weakly overdamped, and what we show is the associated maximum in scattering intensity. For $p = 1.75$ kbar we find $\gamma_T = 0.54(8)$.

Further insight into thermal scaling exponents can be obtained from the staggered magnetic moment, m_s, measured in Ref. 14. Fits to the form $m_s \propto (T_N - T)^{\beta'}$ yield values close to the classical field-theory expectation[27] $\beta' = 0.34$ (XY) or 0.37 [SU(2)]. However, the fit is followed only in a narrow window $T_{SL}(p) < T \leq T_N(p)$, with $T_{SL} \simeq 0.8T_N$ and points further away from the transition diverging clearly from classical scaling[14]. Thus m_s represents very well the scaling relations expected for a narrow CC regime in a system dominated by a QCP [Fig. 4(c)]. The narrow nature of the CC region is also evident in dynamical properties, in that the divergence of the QC and longitudinal mode widths may be used to set dynamical criteria for the crossover from QC to CC

scaling. On the right side of Figs. 3(c), α_L approaches a constant also at finite T, but diverges on approaching $p_c(T)$ (on the left side $\alpha \to 0$ towards the QD regime). In Fig. 3(d), quantum behaviour is evident in the constant values of α reached far from the critical points, a regime including the QC excitations around the line $p = p_c$ (where $\alpha = \alpha_c$). We define classical scaling when $\alpha > 1/2$, and this regime is marked by the shaded regions in Figs. 3(c) and (d). The largely symmetric form of the $\Gamma_{\mathbf{Q}}/\epsilon_{\mathbf{Q}}$ curves is the best available indicator for a classical scaling regime on the disordered side of $T_N(p)$. We have used these parallel static and dynamic approaches to estimate the width of the CC regime in both pressure and temperature, as represented in Fig. 4(c).

Our precise level of control over quantum criticality in $TlCuCl_3$ has inspired recent numerical and analytical studies of the finite-T properties of dimer systems at the coupling-induced QPT. The authors of Ref. 16 argue that $m_s(p)$ and $T_N(p)$ should have the same behaviour, and demonstrate good scaling of m_s with T_N by Quantum Monte Carlo simulations, independent of the functional form in p; this technique cannot address the longitudinal mode. In an effective quantum field theory approach[20], $m_s(p) \propto T_N(p) \propto \sqrt{p - p_c}$ for a linear p-dependence of the exchange couplings, and $\Delta_L(p)$ also has this dependence. This analysis is predicated on proximity to a QCP, but in neglecting the classical critical regime, the field theory does not return the correct behaviour for static quantities around T_N, although its dynamical predictions remain valid. The exchange anisotropy in $TlCuCl_3$ is found[20] to have small quantitative effects on the calculated quantities, but no detectable qualitative ones (*e.g.* on exponents). From our measurements, the best fits to the pressure exponents for m_s and T_N lie close to the classical value of 0.35[14], although the quantum value of 0.5 is not beyond the error bars very close to the QCP. From experiment, the two quantities scale well together near the QCP, as shown in Figs. 4(d) and (e), but depart from universal scaling[16] around an ordered moment of $0.4\mu_B$/Cu [Fig. 4(e)].

We have shown that the effects on the spectrum of quantum and thermal melting are qualitatively very similar. Both result in the systematic evolution of excitations whose gap increases away from the classical phase transition line, rather than simply a loss of coherence due to thermal fluctuations. Microscopically, quantum fluctuations in a dimer-based system cause enhanced singlet formation and loss of interdimer magnetic correlations, while thermal fluctuations act to suppress the spin correlation function $\langle \mathbf{S}_i \cdot \mathbf{S}_j \rangle$ on both the dimer and interdimer bonds. These correlation functions may be estimated from neutron-scattering intensities[23] and also measured in dimerised optical lattices of ultracold fermions[29]. In $TlCuCl_3$, both methods of destroying interdimer coherence cause the triplet modes to evolve in the same way. A key question in the understanding of quantum criticality is whether quantum and thermal fluctuations can be considered as truly independent, and whether this independence may be taken as a definition of the QC regime[16]. Our experimental results suggest that weak departures from universality become detectable at (p, T) values away from the QC and CC regimes, and particularly as we increase the excitation energy, presumably as microscopic details of the fluctuation redistribution cause a mixing of quantum and thermal effects.

Finally, the existence of the longitudinal "Higgs" mode has been questioned in the past. Its visibility has recently been analyzed in detail in the scaling limit[21,28] for systems in two and three dimensions. Our results confirm that it is a genuine example of quantum critical dynamics in three dimensions. Its critical nature makes it infinitely susceptible to thermal fluctuations, so that it becomes overdamped as soon as these become noticeable. While still possessing a significant spectral weight, the longitudinal mode of the pressure-ordered phase is overdamped at finite temperatures, although its critical nature is restored on passing into the finite-T disordered phase. There are several reasons for the ready visibility – in the longitudinal rather than the scalar susceptibility[21] – of the longitudinal mode in $TlCuCl_3$, meaning for the anomalously low value of α_L, despite its critically damped nature. These include the high dimensionality of the system, its low phase space for magnon scattering, the collinearity of the ordered moments, and the fact that one of the spin waves contributing to decay processes is massive. It is reasonable to assume that the same factors also control the anomalously low value of α_c, allowing ready observation of the QC excitations at $p = p_c$ [Figs. 4(a) and (b)], and also the very narrow regime of logarithmic corrections to scaling, which are indiscernible in our data. While logarithmic corrections are expected to be relevant in a system at the upper critical dimension ($d_c = 4$, as here[17]) as p_c is approached[30], the width of the "log-correction" regime is a non-universal quantity. Because our data provide no signs of such corrections in either the thermal or the pressure exponents, we conclude that this regime is unusually small in $TlCuCl_3$. Both the visibility of the longitudinal mode and our level of control over both quantum and thermal fluctuations in $TlCuCl_3$ remain significantly superiour to any other magnetic[17,18], charge-density-wave[31], or cold-atom[32] systems displaying this "Higgs boson."

In summary, high-resolution neutron spectroscopy experiments on the quantum antiferromagnet $TlCuCl_3$ allow us to probe the spin excitations of all phases in and around the QC regime by varying the pressure and temperature. We demonstrate a number of remarkable properties arising at the interface between quantum and classical physics. Quantum and thermal fluctuations have remarkably similar effects in melting the magnetically ordered phase and in opening excitation gaps, but operate quite independently close to the QCP. In the QC regime there is robust ω/T scaling of the energies and widths of critically damped excitations. This scaling crosses over to a classical critical form in a narrow region around the phase transition line $T_N(p)$. The criti-

cally damped longitudinal, or Higgs, mode of the ordered phase is exquisitely sensitive to thermal fluctuations and becomes overdamped in the classical regime.

Materials and Methods

High-quality single crystals of $TlCuCl_3$ were grown by the Bridgman method. INS studies were performed on the cold-neutron triple-axis spectrometer IN14 at the Institut Laue Langevin (ILL). This was operated at constant final wavevector $k_f = 1.15$ Å^{-1}, with a focusing pyrolytic graphite analyser and monochromator, collimation open-60'-open-open and a cooled Be filter positioned between sample and analyser. The temperature and the applied hydrostatic pressure were controlled with a He cryostat and a He gas pressure cell (precision ±50 bar). Spin excitations with longitudinal or transverse polarisation were distinguished unambiguously by working at the wavevector $\mathbf{Q} = (0\ 4\ 0)$, where there are no contributions from mode T_1, while mode T_2 is gapped and evolves with pressure in a different way from mode L. This procedure is described in Ref. 19, where mode T_1 was also measured independently at $\mathbf{Q} = (0\ 0\ 1)$. The intensity measurements for each mode were fitted with a thermal damping Ansatz[33], which has been used for the accurate modelling of phonon damping at finite temperatures[34] and shown in Ref. 22 to be reliable for triplet spin excitations. The magnon is modelled as a damped harmonic oscillator (DHO), whose scattering intensity has the double-Lorentzian lineshape

$$S(\mathbf{Q},\omega) = \frac{A[n(\omega)+1]4\Gamma_{\mathbf{Q}}\epsilon_{\mathbf{Q}}\omega}{[\omega^2 - \epsilon_{\mathrm{DHO}}(\mathbf{Q})^2]^2 + 4\Gamma_{\mathbf{Q}}^2\omega^2}, \qquad (1)$$

where $n(\omega)$ expresses the thermal magnon population. Here $\epsilon_{\mathrm{DHO}}(\mathbf{Q})^2 = \epsilon_{\mathbf{Q}}^2 + \Gamma_{\mathbf{Q}}^2$ is a renormalised energy expressed in terms of the real excitation energy, $\epsilon_{\mathbf{Q}}$, and the linewidth of the scattered intensity, taken as the FWHM, $\Gamma_{\mathbf{Q}}$. The fits presented in Fig. 2 are based on a four-dimensional convolution in momentum and energy of the model cross-section [Eq. (1)] with the instrument resolution, which causes the asymmetric peak shapes. Excitations measured throughout the (p,T) phase diagram were characterised in this way by their energies $\epsilon_{\mathbf{Q}}$, linewidths $\Gamma_{\mathbf{Q}}$, polarisation and intensities [Eq. (1)].

[1] Goldstone, J., Salam, A. & Weinberg, S. Broken Symmetries. *Phys. Rev.* **127**, 965-970 (1962).

[2] Chakravarty, S., Halperin, B. I. & Nelson, D. R. Two-dimensional quantum Heisenberg antiferromagnet at low temperatures. *Phys. Rev. B* **39**, 2344-2371 (1989).

[3] Sachdev, S. *Quantum Phase Transitions* (Cambridge University Press, Cambridge, 2011).

[4] von Löhneysen, H., Rosch, A., Vojta, M. & Wölfle, P. Fermi-liquid instabilities at magnetic quantum phase transitions. *Rev. Mod. Phys.* **79**, 1015-1075 (2007).

[5] Knafo, W., Raymond, S., Lejay, P. & Flouquet, J. Antiferromagnetic criticality at a heavy-fermion quantum phase transition. *Nature Phys.* **5**, 753-757 (2009).

[6] Stockert, O. *et al.* Magnetically driven superconductivity in $CeCu_2Si_2$. *Nature Phys.* **7**, 119-124 (2011).

[7] Bourbonnais, C. & Jérome, D. in *The Physics of Organic Superconductors and Conductors*, ed. Lebed, A. (Springer, Heidelberg, 2008).

[8] Kanoda, K. & Kato, R. Mott Physics in Organic Conductors with Triangular Lattices. *Annu. Rev. Condens. Matter Phys.* **2**, 167-188 (2011).

[9] Bloch, I., Dalibard, J. & Zwerger, W. Many-body physics with ultracold gases. *Rev. Mod. Phys.* **80**, 885-964 (2008).

[10] Zhang, X.-B., Hung, C.-L., Tung, S.-K. & Chin, C. Observation of Quantum Criticality with Ultracold Atoms in Optical Lattices. *Science* **335**, 1070-1072 (2012).

[11] Nikuni, T., Oshikawa, M., Oosawa, A. & Tanaka, H. Bose-Einstein Condensation of Dilute Magnons in $TlCuCl_3$. *Phys. Rev. Lett.* **84**, 5868-5871 (2000).

[12] Giamarchi, T., Rüegg, Ch. & Tchernyshyov, O. *Nature Phys.* **4**, 198-204 (2008), and references therein.

[13] Tanaka, H., Goto, K., Fujisawa, M., Ono, T. & Uwatoko, Y. Magnetic ordering under high pressure in the quantum spin system $TlCuCl_3$. *Physica B* **329-333**, 697-698 (2003).

[14] Rüegg, Ch., Furrer, A., Sheptyakov, D., Strässle, T., Krämer, K. W., Güdel, H. U. & Mélési, L. Pressure-Induced Quantum Phase Transition in the Spin-Liquid $TlCuCl_3$. *Phys. Rev. Lett.* **93**, 257201 (2004).

[15] Matsumoto, M., Normand, B., Rice, T. M., & Sigrist, M. Field- and pressure-induced magnetic quantum phase transitions in $TlCuCl_3$. *Phys. Rev. B* **69**, 054423 (2004).

[16] Jin, S. & Sandvik, A. W. Universal Néel temperature in three-dimensional quantum antiferromagnets. *Phys. Rev. B* **85**, 020409(R) (2012).

[17] Affleck, I. & Wellman, G. F. Longitudinal modes in quasi-one-dimensional antiferromagnets. *Phys. Rev. B* **46**, 8934-8953 (1992).

[18] Lake, B., Tennant, D. A. & Nagler, S. E. Novel Longitudinal Mode in the Coupled Quantum Chain Compound $KCuF_3$. *Phys. Rev. Lett.* **85**, 832-835 (2000).

[19] Rüegg, Ch., Normand, B., Matsumoto, M., Furrer, A., McMorrow, D. F., Krämer, K. W., Güdel, H. U., Gvasaliya, S., Mutka, H. & Boehm, M. Quantum Magnets under Pressure: Controlling Elementary Excitations in $TlCuCl_3$. *Phys. Rev. Lett.* **100**, 205701 (2008).

[20] Oitmaa, J., Kulik, Y. & Sushkov, O. P. Universal finite-temperature properties of a three-dimensional quantum antiferromagnet in the vicinity of a quantum critical point. *Phys. Rev. B* **85**, 144431 (2012).

[21] Podolsky, D., Auerbach, A. & Arovas, D. P. Visibility of the amplitude (Higgs) mode in condensed matter. *Phys. Rev. B* **84**, 174522 (2011).

[22] Rüegg, Ch., Normand, B., Matsumoto, M., Niedermayer, Ch., Furrer, A., Krämer, K. W., Güdel, H. U., Bourges, Ph., Sidis, Y. & Mutka, H. Quantum Statistics of Interacting Dimer Spin Systems. *Phys. Rev. Lett.* **95**, 267201 (2005).

[23] Normand, B. & Rüegg, Ch. Complete bond-operator theory of the two-chain spin ladder. *Phys. Rev. B* **83**, 054415 (2011), and references therein.

[24] Shevchenko, P. V., Sandvik, A. W. & Sushkov, O. P. Double-layer Heisenberg antiferromagnet at finite temperature: Brueckner Theory and Quantum Monte Carlo simulations. *Phys. Rev. B* **61**, 3475-3487 (2000).

[25] Oosawa, A., Kakurai, K., Osakabe, T., Nakamura, M., Takeda, M. & Tanaka, H. Pressure-Induced Successive Magnetic Phase Transitions in the Spin Gap System $TlCuCl_3$. *J. Phys. Soc. Jpn.* **73**, 1446-1449 (2004).

[26] Sachdev, S. Quantum Theory of Condensed Matter, presented at 24th Solvay Conference on Physics, Brussels, Oct 2008. Available at <http://arxiv.org/abs/cond-mat/0901.4103> (2009).

[27] Zinn-Justin, J. *Quantum Field Theory and Critical Phenomena* (Oxford University Press, Oxford, 2002).

[28] Podolsky, D. & S. Sachdev, S. Spectral functions of the Higgs mode near two-dimensional quantum critical points. *Phys. Rev. B* **86**, 054508 (2012).

[29] Greif, D., Uehlinger, T., Jotzu, G., Tarruell, L. & Esslinger, T. Short-Range Quantum Magnetism of Ultracold Fermions in an Optical Lattice. *Science* **340**, 1307-1310 (2013).

[30] Kulik, Y. & Sushkov, O. P. Width of the longitudinal magnon in the vicinity of the O(3) quantum critical point. *Phys. Rev. B* **84**, 134418 (2012).

[31] Littlewood, P. B. & Varma, C. M. Gauge-Invariant Theory of the Dynamical Interaction of Charge Density Waves and Superconductivity. *Phys. Rev. Lett.* **47**, 811-814 (1981).

[32] Endres, M. *et al.* The 'Higgs' amplitude mode at the two-dimensional superfluid/Mott insulator transition. *Nature* **487**, 454-458 (2012).

[33] Talbot, E. F., Glyde, H. R., Stirling, W. G. & Svensson, E. C. Temperature dependence of $S(\mathbf{Q}, \omega)$ in liquid ^{4}He under pressure. *Phys. Rev. B* **38**, 11229-11244 (1988).

[34] Fåk, B. & Dorner, B. Phonon line shapes and excitation energies. *Physica B* **234-236**, 1107-1108 (1997).

Acknowledgements

We are grateful to S. Sachdev, A. Sandvik and especially M. Vojta for helpful comments. We thank the sample environment team at the ILL, where these measurements were performed, for their assistance. This work was supported by the EPSRC, the Royal Society, the Swiss NSF, and the NSF of China under Grant No. 11174365.

Author contributions

P.M. and Ch.R. carried out the experiments with the help of instrument scientist M.B. $TlCuCl_3$ single crystals were synthesised by K.W.K. The theoretical and experimental framework was conceived by Ch.R., D.F.M. and B.N. Data refinement and figure preparation were performed by P.M. and Ch.R. The text was written by B.N. and Ch.R.

Additional information

Reprints and permissions information is available at www.nature.com/reprints. The authors declare no competing financial interests. Correspondence and requests for materials should be addressed to Ch.R. (christian.rueegg@psi.ch).